Surfaces and Interfaces 55 (2024) 105294

Contents lists available at ScienceDirect

Surfaces and Interfaces

journal homepage: www.sciencedirect.com/journal/surfaces-and-interfaces

Role of zwitterionic lipid headgroups on monolayer formation and interfacial dilatational rheology in binary mixtures of phospholipids and cholesterol: A pendant drop tensiometer study

Andrew R. White [a], Monica Iepure [a], Jonathan Arredondo [a], Maryam Darwish [a], Chidubem Onyeagoro [a], Younjin Min [a,b,*]

[a] Department of Chemical and Environmental Engineering, University of California, Riverside, CA 92521, USA
[b] Material Science and Engineering Program, University of California, Riverside, 92521 CA, USA

ARTICLE INFO

Keywords:
Zwitterionic phospholipids
Cholesterol
Pendant drop tensiometer
Gibbs free energy of mixing
Interfacial rheology

ABSTRACT

The complex composition of biological membranes, comprising a diverse array of lipids with unique moieties, has garnered increased attention due to the recognized roles of lipids in membrane stability and biological processes. Even subtle changes in phospholipid headgroups and fatty acyl tails profoundly affect the formation and interfacial dynamics of lipid monolayers at the air-water interface. However, the molecular-level understanding of their intermolecular forces and interactions during these processes, directly relating to the lipid chemical structures, is not well-explored. To better understand these complex physicochemical phenomena, simplified model monolayers with precise control over lipid types and compositions are utilized. In this study, we employ the pendant drop tensiometer technique to investigate the formation and interfacial rheology of 1,2-dipalmitoyl-sn-glycero-3-phosphocholine (DPPC) and 1,2-dipalmitoyl-sn-glycero-3-phosphoethanolamine (DPPE) monolayers, with varying amounts of cholesterol (CHOL) for the first time. These two phospholipids, with identical C16:0 acyl tails but different headgroups, exhibit marked differences in their interfacial interactions with CHOL and water molecules, consequently affecting monolayer formation and rheology. In the absence of CHOL, DPPE monolayers typically display a lower dilatational modulus than DPPC, attributed to increased headgroup hydration. However, introducing CHOL reverses this trend, resulting in stiffer DPPE-CHOL monolayers compared to DPPC-CHOL. With CHOL, we observe its well-known condensation effect on DPPC monolayers, yet for DPPE monolayers, both condensation and expansion effects are noted, contingent on CHOL amount. We anticipate this work will not only deepen our fundamental understanding of the structure-composition-property relationships in lipid molecules but also provide a robust foundation for comprehending more intricate biological systems.

1. Introduction

Lipids are the primary building blocks of biological membranes. They come in many varieties, including the categories of glycerophospholipids, sphingolipids, and sterols [1], and serve important roles in membrane structures and functions [2]. Specific combinations of these lipids lead to the formation of nano- and micro-domains, commonly referred to as “lipid rafts” [3–6], which play key roles in cell signaling, the adsorption of specific proteins, membrane stability, and changes in mechanical properties [6,7] in a wide range of biological membranes, from the myelin sheath [8,9] to cancer cells [10–12].

Glycerophospholipids consist of a glycerol with a phosphoric acid and two fatty acids attached as esters. Within this class, phosphatidylcholines (PC) and phosphatidylethanolamines (PE) are the most abundant lipids in mammalian cells, making up 45-55% and 15-25%, respectively, of the total lipid composition [13]. Sterols are similarly abundant and contribute to the matrix of cellular membranes (mammalian cells contain one major type of sterol, i.e., cholesterol,

Abbreviations: DPPC, 1,2-dipalmitoyl-sn-glycero-3-phosphocholine; DPPE, 1,2-dipalmitoyl-sn-glycero-3-phosphoethanolamine;, Cholesterol:CHOL; PC, Phosphatidylcholines; PE, Phosphatidylethanolamines; X_{CHOL}, CHOL mole fractions; PTFE, Polytetrafluoroethylene.

* Corresponding author at: Department of Chemical and Environmental Engineering, University of California, Riverside, CA 92521, USA.
E-mail address: ymin@engr.ucr.edu (Y. Min).

https://doi.org/10.1016/j.surfin.2024.105294
Received 5 June 2024; Received in revised form 14 October 2024; Accepted 16 October 2024
Available online 18 October 2024

consisting of 10-20% of lipid components) [13]. The molecular structures of commonly encountered PC and PE lipids, 1,2-dipalmitoyl-sn--glycero-3-phosphocholine (DPPC) and 1,2-dipalmitoyl-sn-glycero-3-phosphoethanolamine (DPPE), as well as cholesterol (CHOL), are shown in Fig. 1. Both DPPC and DPPE have the same hydrocarbon chain length in hydrophobic tails (i.e., C16:0 acyl tails) but differ in their zwitterionic headgroups: phosphatidylcholine (PC) versus phosphatidylethanolamine (PE), respectively. Cholesterol has a short alkyl side chain and a hydroxy group attached to a steroid nucleus ring structure. In bilayers, these lipids arrange themselves with their hydrophilic sides outside the bilayer and their hydrophobic sides within. Similarly, in monolayers at an air-water interface, the hydrophilic groups are in the aqueous phase, while the hydrophobic portions extend into the air. When placed side by side, these lipids exhibit complicated intermolecular forces, including hydrogen bonding, steric, electrostatic, hydrophobic, and van der Waals interactions, which, in turn, dictate the formation, structure, and mechanical properties of the resulting biomembranes in the form of either bilayers or monolayers [3,14–16]. Even a subtle change in the structure of hydrophilic headgroups in DPPC and DPPE (See Figs. 1A and B) leads to different modes of intermolecular interactions. In addition to attractive interactions (favorable van der Waals interactions) and repulsive interactions (steric and electrostatic interactions) laterally arising among the headgroup molecules, the PE headgroup is found to serve both as a hydrogen bond acceptor and donor, whereas the PC headgroup can only act as an acceptor. This difference leads to DPPE lipids exhibiting a higher degree of hydration over DPPC lipids at air-water interfaces [17], as well as stronger hydrogen bonding interactions between neighboring DPPE molecules in lipid membranes [18]. In a study comparing the interfacial dilatation rheology of DPPC and DPPE monolayers, the increased hydration of DPPE and its reduced monolayer cohesion led to a lower elastic modulus than DPPC lipids when the acyl tails were symmetric [19].

CHOL exhibits strong interactions with these phospholipids, i.e., DPPC and DPPE when integrated into monolayers and bilayers [20,21]. In general, the hydroxy group of CHOL has the capacity to form robust hydrogen bonds with adjacent phospholipid headgroups [21–23], and its nonpolar ring structure and alkyl tail also favorably interact with the acyl tails of phospholipids [2]. Furthermore, CHOL has been demonstrated to impose a dehydrating effect on phospholipid membranes when incorporated [24]. Due to the aforementioned differences in chemical structures and resultant intermolecular interactions arising between neighboring headgroups in PC and PE lipid molecules, there become noticeable distinctions in their respective interactions with CHOL. Stronger inter-headgroup hydrogen bonding in DPPE lipids favors phospholipid-phospholipid over phospholipid-cholesterol interactions more prominently than in DPPC-CHOL films, leading to distinctive alternations in miscibility, phase transition temperature, and, consequently, the population and size of nano- and microdomains (rafts) [18]. CHOL has been observed to be miscible with DPPC membranes, primarily due to the so-called condensation effect. This effect enhances the orientation order of DPPC molecules with respect to the horizontal air-water interface, thereby reducing the area per lipid molecule [2, 25–33]. In contrast, the miscibility of CHOL with DPPE membranes strongly depends on the hydrophobic chain length, degree of (un) saturation in the acyl tails of DPPE lipid molecules, and the relative amount of CHOL present. In general, increasing the phospholipid acyl chain length and the amount of CHOL tends to favor the formation of CHOL-poor domains in DPPE membranes [18].

Although previous studies have heavily highlighted the complex interactions between phospholipids involving DPPC and DPPE and cholesterol, corresponding research findings are rather controversial, in particular, for the case of DPPE and cholesterol binary mixture. For instance, some of the monolayer studies involving DPPE-CHOL films, conducted using a Langmuir trough [28,34], have reported that the

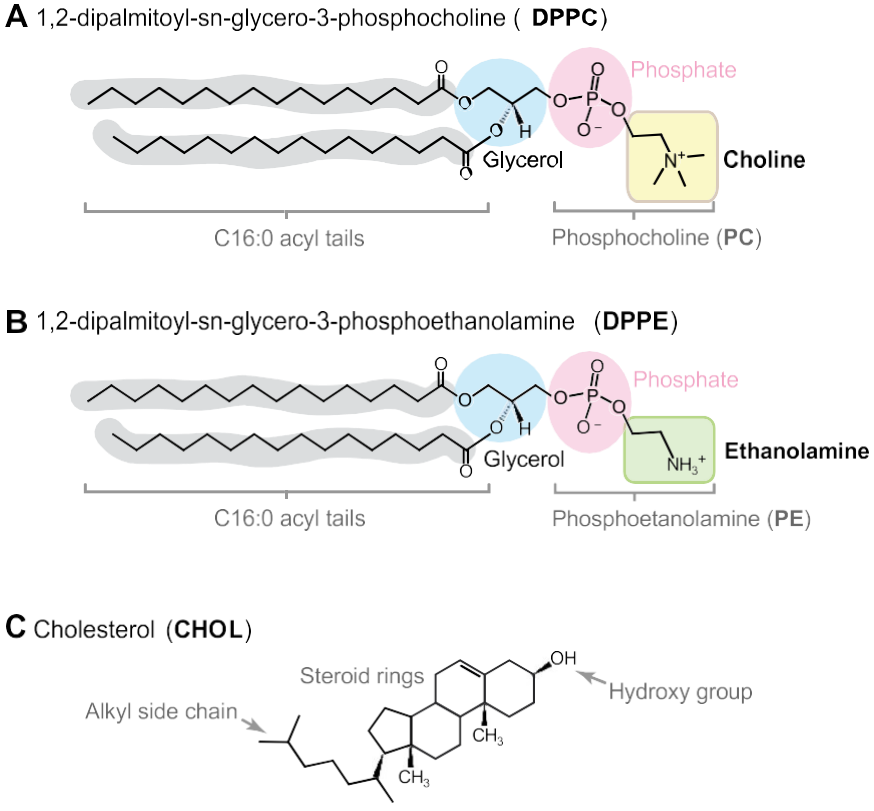

Fig. 1. Molecular structures of **(A)** 1,2-dipalmitoyl-sn-glycero-3-phosphocholine (DPPC), **(B)** 1,2-dipalmitoyl-sn-glycero-3-phosphoethanolamine (DPPE), and **(C)** cholesterol (CHOL).

addition of CHOL to DPPE monolayers results in an expansion effect on the mean molecular areas at low CHOL mole fractions (X_{CHOL}) while a condensation effect is observed at relatively high X_{CHOL} values (e.g., at $X_{CHOL} \approx 0.3$ or so) with the specific value depending on the degree of compressibility of monolayers. In contrast, Korchowiec et.al [35] have found the opposite trend where the condensation effect takes place when X_{CHOL} is at or below 0.4 while the expansion effect occurs when $X_{CHOL}$is greater than 0.5 which are consistent with observations from ref. [18].

Furthermore, surprisingly, there has been little attention given to the apparent relationships among chemical structures, molecular organizations, and physicochemical properties, particularly in the context of lipid membrane mechanics and interfacial rheological behaviors. There are some studies reporting how CHOL can modulate the elastic modulus and viscosity of DPPC monolayers [36] and their corresponding phase transition behaviors as a function of hydrophobic chain lengths [37]. However, no literature is available that delineates the effects of CHOL on DPPE monolayers and how it alters DPPE membrane interactions and stiffness. Consequently, no systematic studies have been reported to elucidate not only the effects of lipid chemical structures (PC vs. PE) but also the qualitative and quantitative effects of CHOL on their emerging intermolecular interactions and mechanical properties.

The aims of this present study are to investigate the effects of PC versus PE headgroups on the interfacial rheology of binary mixed phospholipid-CHOL monolayers, and to provide a comprehensive comparison of how subtle changes in lipid chemical structures, such as, headgroups, can thermodynamically impact the formation of monolayers at the air-water interface, for the first time. To achieve these goals, two types of phospholipids, i.e., DPPC and DPPE are studied in the form of monolayers in the absence and presence of CHOL using a pendant drop tensiometry [37–41]. Set of surface pressure-area isotherms is constructed with precise attention to detail to determine whether changes in the amount of CHOL on lipid monolayers affect the intramembrane interactions and resulting thermodynamic properties including the excess Gibbs free energy of mixing are extracted. We compare the interfacial rheological responses of DPPC-CHOL and of DPPE-CHOL binary mixtures in the form of monolayers that reflect their chemical structure and composition. This comprehensive approach is expected to shed a light on understanding of how changes on key lipid compositions may affect intra- as well as intermembrane interactions, consequently influencing membrane stability and fluidity.

2. Materials and methods

The lipids used were 1,2-dipalmitoyl-sn-glycero-3-phosphocholine (DPPC) (synthetic, Avanti 850355, >99%) (MW = 734.039 g/mol), 1,2-dipalmitoyl-sn-glycero-3-phosphoethanolamine (DPPE) (synthetic, Avanti 850705, >99%) (MW = 691.959 g/mol), and cholesterol (CHOL) (ovine wool, >98%) (MW = 386.654 g/mol), all purchased from Avanti Polar Lipids and used as received. Mixtures of DPPC:CHOL with CHOL mole fractions, X_{CHOL} = 0,0.1,0.2,…,1 and concentration 0.1 mg/ml were prepared in HPLC grade chloroform (Fisher). Mixtures of DPPE: CHOL with X_{CHOL} = 0,0.1,0.2,…,1 and concentration 0.1 mg/ml were prepared in 3:1 v/v chloroform : methanol. The aqueous phase for all measurements was phosphate buffered saline (PBS) (Sigma) with 10 mM phosphate, 2.7 mM KCl, and 137 mM NaCl and at pH 7.4.

Both surface pressure versus area isotherms and interfacial dilatational rheology were performed using an optical pendant drop tensiometer (Attension Theta, Biolin Scientific). The setup used a syringe pump with a 1 ml glass syringe (Hamilton) to dispense and suspend a PBS drop from a 1.57 mm outer diameter polytetrafluoroethylene (PTFE) capillary. The end of the PTFE capillary was surrounded by air but within a quartz cuvette that was partially filled with water, and the opening of the cuvette was sealed with Parafilm. This created a saturated atmosphere within the cuvette and limited evaporation of the PBS drop during measurements. The liquid path additionally contained a piezoelectric membrane (Attension PD200, Biolin Scientific) which could be actuated sinusoidally with specified frequency and amplitude to precisely vary the drop volume for dilatational rheology. All measurements were performed at 23 ± 1°C.

For surface pressure versus area isotherms, first an approximately 16 μl drop of PBS was suspended from the PTFE capillary. The measured PBS surface tension was 72.9 ± 0.2 mN/m. Then, through a small hole in the Parafilm sealing the cuvette, between 0.3-0.4 μl (depending on the lipid mixture) of a 0.1 mg/ml lipid mixture was very carefully deposited directly onto the drop surface using a 0.5 μl glass syringe (Hamilton) such that the surface tension was practically unchanged. Five minutes elapsed to allow the spreading solvent to evaporate, and the small hole in the Parafilm seal was sealed. Then using the syringe pump, the drop volume was decreased such that the surface area decreased at approximately 0.02 mm²/s while recording images of the drop at 1 frame per second. The images were then analyzed in commercial software (OneAttension, Biolin Scientific) by fitting the Young-Laplace equation to each drop shape to determine γ as well as the surface area A. The Bond numbers remained between $0.15 < Bo^* < 0.5$ during volume reduction. Knowing A and the precise volume of lipid mixture added, the mean molecular area a was also calculated.

Interfacial dilatational rheology was performed using the oscillating pendant drop method. Again, an approximately 16 μl drop of PBS was first suspended from the PTFE capillary, and between 0.3-0.4 μl of a 0.1 mg/ml lipid mixture was deposited onto the drop surface. After waiting 5 min for the spreading solvent to evaporate, the drop volume was decreased using the syringe pump until Π = 5 mN/m. At this fixed surface pressure, the drop oscillated at frequencies between 0.01-1 Hz for 5-10 periods with amplitude ΔA = 1% which was determined to be within the linear viscoelastic region. After completing the frequency sweep, the drop volume was decreased again until Π = 10 mN/m and another frequency sweep was made. A frequency sweep was performed at each surface pressure between 5 to 40 mN/m in increments of 5 mN/m. After each adjustment of Π, typically 10-15 min were required to achieve an equilibrium surface tension. Images of the oscillating pendant drops were again analyzed in the same commercial software to determine γ and A. The $\gamma(t)$ and $A(t)$ data were analyzed using an in-house MATLAB script to determine the dilatational modulus and phase angle as discussed in the Analysis section.

3. Analysis

3.1. Thermodynamic analysis of mixed binary monolayers

A fixed number of molecules n_1 and n_2 of components 1 and 2, respectively, is added to an aqueous-air interface, and each component occupies a portion of the total surface area A_1 and A_2. Each component has a corresponding average area per molecule $a_i = A_i/ n_i$ where the subscript i is either 1 or 2. Initially a_i is large such that the surface pressure $\Pi = \gamma_o - \gamma$, where γ_o and γ are the surface tensions of the subphase in the absence and presence of monolayers respectively, is approximately zero. As the monolayer is compressed, Π generally increases. For an ideal monolayer with two non-interacting components, the average area per molecule $a_{12,\,ideal}$ at a fixed Π and temperature T is simply additive based on the respective areas per molecule of the components and their corresponding mole fractions, X_1 and X_2:

$$a_{12,ideal} = X_1 a_1 + X_2 a_2. \quad (1)$$

In a real binary monolayer, intermolecular forces between the two components can lead to the condensation or expansion of the average area per molecule (a_{12}) relative to the ideal case (i.e., $a_{12,\,ideal}$), leading to an average excess area per molecule a_{ex}:

$$a_{ex} = a_{12} - (X_1 a_1 + X_2 a_2), \quad (2)$$

which can be easily measured directly from $\Pi - a$ isotherms. A negative

a_{ex} indicates condensation of the monolayer, while a positive a_{ex} indicates expansion relative to the ideal monolayer case.

The corresponding excess free energy of mixing during monolayer formation can be calculated by considering the Gibbs free energy per mole, G. As the Gibbs free energy per mole can be defined in terms of independent variables temperature T, pressure P, surface tension γ, and number of moles of the i^{th} component n_i, the corresponding change in free energy becomes $dG = -SdT + VdP - ad\gamma + \sum \mu_i dn_i$ where S is entropy, V is volume, and μ_i is the chemical potential of the i^{th} component. For changes only in γ, this becomes $dG = -ad\gamma$, or equivalently in terms of surface pressure, i.e., Π:

$$dG = ad\Pi. \tag{3}$$

Similarly, in an ideal monolayer with no interactions between the components of 1 and 2, the corresponding free energy ($G_{12,\ ideal}$) becomes additive such that $G_{12,ideal} = X_1G_1 + X_2G_2$.In a real monolayer, there is some excess energy $G_{ex} = G_{12} - G_{12,ideal}$. Eq. 3 can be used to derive an expression for G_{ex} which can be calculated directly from $\Pi - a$ isotherms [42]:

$$\Delta G_{ex} = \int_0^{\Pi} a_{ex} d\Pi. \tag{4}$$

Details on the derivation of Eq. 4, originally from Ref. [42], are included in the **Supplementary information**. At a given Π, a negative ΔG_{ex} indicates net attraction between the two interacting components while a positive ΔG_{ex} indicates net repulsion and a less stable monolayer.

3.2. Surface Tension Measurement

Surface tension for both $\Pi - a$ isotherms and dilatational rheology is measured using the pendant drop method [43,44] from the family of axisymmetric drop shape analysis (ADSA) techniques [45]. Briefly, the shape of a pendant drop suspended from a capillary with isotropic surface tension is dictated by the balance of gravity deforming the drop surface and surface tension resisting the deformation, as described by the Young-Laplace equation, $2\gamma H = \Delta\rho gz - (2\gamma/R)$, where H is the mean curvature of the drop surface, $\Delta\rho$ is the density difference between the drop and surrounding air, z is the elevation height, and R is the radius of curvature at the drop apex (Fig. 2A). Using R as a characteristic length scale, the dimensionless Young-Laplace equation becomes:

$$2H^* = \mathrm{Bo}^* z^* - 2, \tag{5}$$

where '*' indicates dimensionless quantities and $\mathrm{Bo}^* = \Delta\rho gR^2/\gamma$is the Bond number relating the influence of gravity (numerator) and surface tension (denominator). In practice, Eq. 5 is parameterized with respect to an arc length s in the meridional plane and the surface tangent angle ψ (see Fig. 2A), resulting in three coupled differential equations that are solved numerically, the details of which can be found in many references [45–48]. The magnitude of Bo* is important in the fitting of Eq. 5 to the shape of pendant drops. WhenBo*is small, γ dominates the shape of the pendant drop which tends toward a spherical shape to minimize surface area. In such a situation it is difficult for a fitting algorithm to satisfactorily fit the Young-Laplace equation and substantial errors in γ result. Generally, it is necessary for Bo* > 0.15 for many algorithms to properly fit the Young-Laplace equation [46], although some algorithms have been successful for Bo* < 0.1 [47].

3.3. Interfacial Dilatational Rheology

With an insoluble monolayer adsorbed onto the pendant drop surface, we modulate the surface area of droplet by varying the drop volume sinusoidally. If the surface area deformation is only dilatational, we would impose an area change ΔA while preserving the shape of the droplet (see the "left" schematic of Fig. 2B). However, due to the drop being non-spherical, the surface area will undergo combined dilatation and shear as shown in the "right" schematic of Fig. 2B. If the insoluble monolayer is capable of resisting only dilatational deformation, the Young-Laplace equation is valid and can be used to measure the instantaneous surface tension of the monolayer during deformation [49]. On the other hand, if the monolayer can also resist shear deformation along with dilatational deformation, additional in-plane shear stresses will develop and invalidate the use of the Young-Laplace equation, although the Young-Laplace equation can still appear to fit the drop shape properly in these situations [50]. This is an important note since, in our measurements for some monolayers, a negative phase shift between temporal changes in γ and A (i.e., $\gamma(t)$ and $A(t)$ respectively) indeed appears, suggesting that shear resistance phenomena may still take place in some cases although the Young-Laplace equation fits well to experimental images as discussed in more detail in the

Continuing with the assumption that the monolayer resists only dilatational deformation, and the surface area deformation is approximately planar, for small deformations, the change in the surface tension corresponding to changes in surface area is characterized by the dilatational modulus E [51,52]:

$$E = A_e \frac{\Delta\gamma}{\Delta A}, \tag{6}$$

where A_e is the surface area at equilibrium before oscillation, ΔA is the (±) area change. The rationale beyond this equation is that as we vary

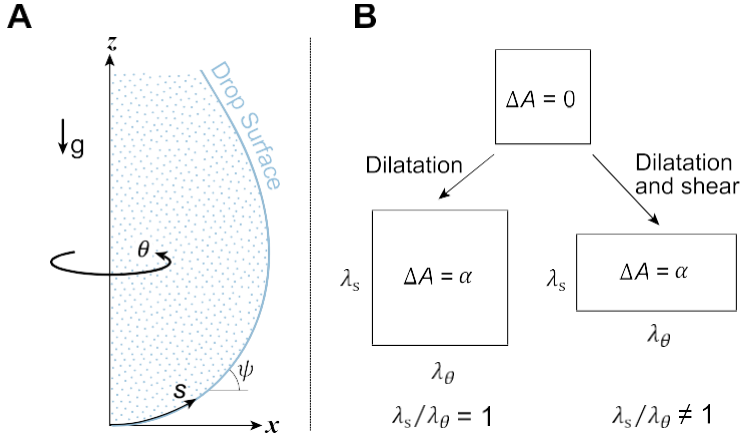

Fig. 2. The two relevant coordinate systems for axisymmetric drop shape analysis, (x, z, θ) and (s, ψ), are shown in **(A)**. In **(B)**, graphical representations of dilatational deformation with area change $\Delta A \neq 0$ (= α) and combined dilatational and shear deformation are shown, where λ_s and λ_θ are the strains in the meridional and azimuthal directions, respectively.

the volume sinusoidally, the volume changes are small such that the area also changes approximately sinusoidally:

$$A(t) = A_e + \Delta A\sin(2\pi ft), \quad (7)$$

where f is the oscillation frequency. If the corresponding surface tension response is linear, it will likewise be sinusoidal:

$$\gamma(t) = \gamma_e + \Delta\gamma\sin(2\pi ft + \phi), \quad (8)$$

where γ_e is the surface tension at equilibrium, $\Delta\gamma$ is the (±) change in γ, and ϕ is the phase angle. If the monolayer is purely elastic, $\gamma(t)$ and $A(t)$ will be in phase (ϕ =0), and if the monolayer is viscoelastic there will be some positive phase shift $0 < \phi < 90^o$, with $\phi = 90^o$ being a purely viscous monolayer.

The amplitudes $\Delta\gamma$ and ΔA and the phase angle ϕ are determined by applying a discrete Fourier transform to the $\gamma(t)$ and $A(t)$ signals [53]. Additionally, the dilatational modulus can be decomposed into a real and imaginary component:

$$E = |E|e^{i\phi} = E' + iE'', \quad (9)$$

where the real component E' is the storage or elastic modulus, and the imaginary component E'' is the loss or viscous modulus. The dilatational elasticity and viscosity are then $\varepsilon = E'$ and $\kappa = E''/2\pi f$, respectively.

4. Results and discussion

4.1. Monolayer formation

The surface pressure versus mean molecular area during the constant rate compression of the monolayers is shown in Figs. 3A and B for DPPC-CHOL and DPPE-CHOL binary mixtures, respectively. The DPPC-CHOL isotherms are in approximate agreement with similar measurements made with Langmuir troughs in previous studies [25–30]. In these prior studies, the molecular area at which the surface pressure first becomes non-zero ranges from near 110 Å² [25,26] to near 90 Å² [28,29] as we have observed. The collapse pressure for DPPC in Fig. 3A occurs at about Π = 60 mN/m and a molecular area near 43 Å². The plateau in our DPPC isotherm is less defined in the vicinity of Π = 10 mN/m where liquid expanded (LE) and liquid condensed (LC) phases should coexist. The lack of a well-defined plateau has been observed in other pendant drop and bubble studies [38,39,41], and A. Jyoti et al. [38] demonstrated the sensitivity of the presence of an approximate plateau could depend on how the lipids were deposited onto the drop surface. The CHOL isotherm in Fig. 3A shows that the area at which Π begins increasing is about 37 Å², and there is a rapid increase in Π thereafter, indicative of good agreements with previous results [28,29]. In Fig. 3A, the isotherms with mixtures of DPPC and CHOL generally fall between the DPPC (-◦-) and CHOL (-◦-) isotherms according to X_{CHOL}. These mixed monolayers will be further analyzed in more detail below, including the aspects of excess areas (a_{ex}: Fig. 4) and excess mixing energy (G_{ex}: Fig. 5).

There are fewer examples of DPPE-CHOL monolayers reported in the literature. The mean molecular area at which Π becomes nonzero varies considerably in the few studies of DPPE-CHOL binary mixtures, from approximately 50 Å² (on water, 100 mM NaCl, and 33 mM $CaCl_2$ subphases) [35] to 80 Å² (on water) [34]. In our measurement (Fig. 3B), the mean area where Π becomes nonzero appears a slightly less at about 45 Å², which may be attributed to the presence of mixtures of salts in our subphase. Our subphase is PBS with 10 mM phosphate, 2.7 mM KCl, and 137 mM NaCl and such high ionic strengths contributes to decrease net repulsive interactions, possibly arising between zwitterionic PE headgroups, leading to a tighter packing. The addition of CHOL to DPPE monolayers has pronounced yet non-monotonic effects on the mean molecular areas: interestingly, at higher Π values, DPPE-CHOL isotherms with higher X_{CHOL} values (indicated by green shades: X_{CHOL} = 0.6 – 0.9) actually exhibit larger molecular areas compared to those with lower X_{CHOL} values (indicated by blue shades: X_{CHOL} = 0.1 – 0.5). This notable contrast with DPPC-CHOL isotherms can be attributed to the significant impacts of the PE headgroups on interactions with CHOL, which we will discuss in more detail next.

In order to elucidate the fundamental roles of zwitterionic lipid headgroups on their respective molecular interactions in the form of monolayers, the excess mean molecular area (a_{ex}) shown in Fig. 4 was calculated using the isotherms presented in Fig. 3 and Eqs. 1-2. The ratio $a_{ex}/a_{12,ideal}$, representing the relative condensation ($a_{ex}/a_{12,ideal} < 0$) or expansion ($a_{ex}/a_{12,ideal} > 0$) of the molecular area for both binary mixtures of DPPC-CHOL and DPPE- CHOL, is plotted as a function of CHOL mole fraction (X_{CHOL}) and shown in Fig. 4. In Fig. 4A, the addition of CHOL into DPPC monolayers leads to significant condensation, with the maximum effect occurring between $0.4 < X_{CHOL} < 0.7$ and the relative magnitude of the condensation increasing with decreasing Π. This condensation effect for all X_{CHOL} is in agreement with similar studies where DPPC-CHOL monolayers were investigated [25–30]. In these monolayers, the steroid rings and alkyl tail in CHOL can interact with the acyl tails in DPPC, increasing the orientation order of lipid molecules which reduces the area occupied by each lipid as a result. Furthermore, the small molecular size of cholesterol enables it to fill

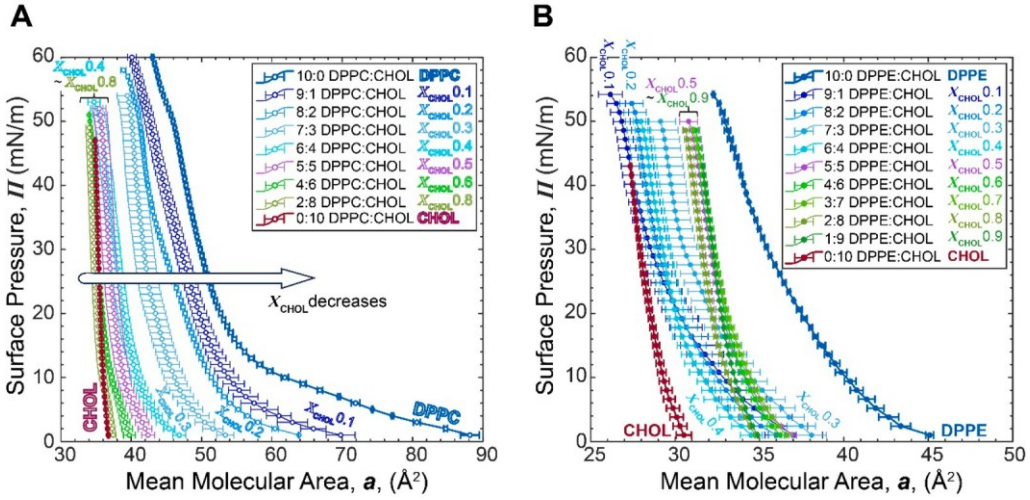

Fig. 3. Surface pressure versus area isotherms are plotted for **(A)** DPPC-CHOL and **(B)** DPPE-CHOL monolayers. Isotherms for each lipid mixture were performed in duplicate, with the horizontal error bars representing ± one standard deviation in the mean molecular area for each surface pressure. DPPC : CHOL mixtures of 3:7 and 1:9 are omitted from **(A)** for clarity.

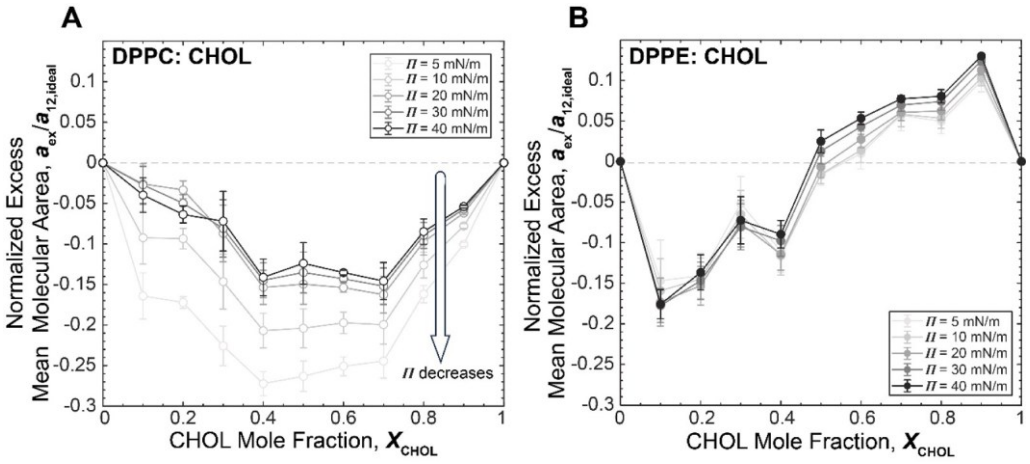

Fig. 4. The excess mean molecular area divided by the ideal mean molecular area for **(A)** DPPC-CHOL and **(B)** DPPE-CHOL monolayers are plotted versus CHOL mole fraction for **Π** = 5, 10, 20, 30, and 40 mN/m. The error bars represent ± one standard deviation based on the duplicated surface pressure versus area isotherms.

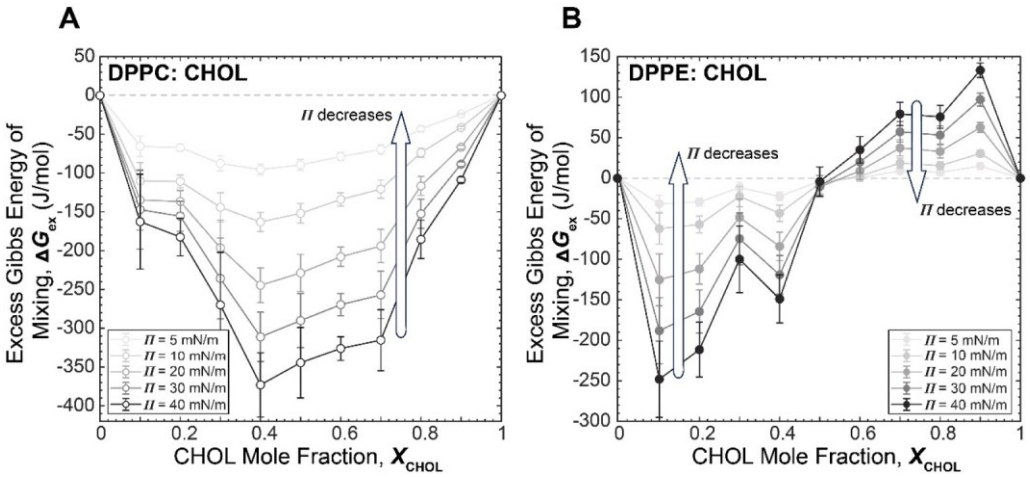

Fig. 5. The excess Gibbs energy of mixing for **(A)** DPPC-CHOL and **(B)** DPPE-CHOL monolayers versus CHOL mole fraction are plotted for **Π** = 5, 10, 20, 30, and 40 mN/m. The error bars represent ± one standard deviation based on the duplicated surface pressure versus area isotherms.

voids in the monolayer that otherwise would be too small for DPPC, further reducing the effective area per lipid [2]. It is worth noting that our results show some differences with some earlier Langmuir monolayer studies, particularly for DPPC/CHOL mixtures. While Langmuir studies typically report the minimum excess area (maximum interaction) at X_{CHOL} = 0.25 or 0.5, our data shows this occurring at X_{CHOL} = 0.4 [54,55]. This difference could be attributed to our use of PBS buffer instead of pure water, which may alter lipid-lipid and lipid-cholesterol interactions due to electrolyte screening effects.

Comparing $a_{ex}/a_{12,ideal}$ for DPPE-CHOL (Fig. 4B) with that of DPPC-CHOL demonstrates a significant shift in behavior. Notable condensation is observed for $X_{CHOL} < 0.5$, which remains relatively consistent across the range of pressures studied (**Π** = 5 – 40 mN/m). However, for $X_{CHOL} > 0.5$, a clear expansion effect is observed, with the area occupied by each lipid being as 10% greater than that of an ideal monolayer. This suggests some unfavorable interactions between CHOL and DPPE at larger X_{CHOL} values, which can be further analyzed by calculating the excess Gibbs free energy of mixing.

Using the **Π** - ***a*** isotherms from Fig. 3 in conjunction with Eq. 4, the excess mixing energy, ΔG_{ex}, was calculated using Eq. 4, and is plotted in Fig. 5 as a function of X_{CHOL}. This quantity represents the change in energy required to form the mixed monolayer, relative to ideal mixing between the two lipids present in the monolayer. In Fig. 5A, ΔG_{ex} is negative for all values of X_{CHOL} and across all ***Π***, indicating a reduction in the energy required to form the monolayer due to net attraction between DPPC and CHOL. This net attraction can arise from a combination of inter-headgroup hydrogen bonding between DPPC and CHOL, as well as hydrophobic interactions between the acyl tail of DPPC and the ring structure and alkyl tail of CHOL (See Fig. 1) [2,22]. The hydrogen bonding between the two lipids has the additional effect of displacing water that was previously hydrating the PC headgroup, further reducing the area per lipid [24]. As ***Π*** increases, the distance between lipids decreases, leading to stronger attractive interactions and a more negative ΔG_{ex}. Due to the presence of its amine group, DPPE is capable of being both a hydrogen bond donor and acceptor, in contrast to DPPC only being an acceptor. This distinction leads to two major implications for the behavior of the PE headgroup compared to the PC headgroup: increased hydration of the PE headgroup [17,18] and more favorable phospholipid-phospholipid inter-headgroup interactions. These differences aid in interpreting the ΔG_{ex} results for DPPE-CHOL monolayers shown in Fig. 5B. For $X_{CHOL} < 0.5$, ΔG_{ex} is negative indicating net attraction between DPPE and CHOL. Like with DPPC, these interactions can include inter-headgroup bonding between DPPE and CHOL and well as hydrophobic interactions. However, as X_{CHOL} is approaching 0.5, ΔG_{ex} tends toward zero, which signifies a reduction in favorable interactions between DPPE and CHOL with the increasing addition of

CHOL. A plausible explanation for this behavior is that the stronger inter-headgroup hydrogen bonding and electrostatic interactions between DPPE molecules makes DPPE-DPPE interactions more favorable than DPPE-CHOL interactions [18,56]. At very low X_{CHOL}, CHOL may be able to induce a degree of dehydration and occupy voids in the DPPE-rich monolayer which reduces the area per lipid, but this effect encounters diminishing returns as X_{CHOL} increases due to suboptimal interactions between CHOL and DPPE. For $X_{CHOL} > 0.5$ (See Fig. 5B), ΔG_{ex} becomes positive, indicating a net repulsion between CHOL and DPPE and an increase in immiscibility, especially in the gel state, i.e., a more positive ΔG_{ex} is observed at higher Π. In this range, it is plausible that distinct DPPE-rich domains exist within an otherwise CHOL-rich monolayer, aligning with previous experimental observations [18,57]. Analogous to how increased packing density amplified net-attractive interactions between DPPE and CHOL for $X_{CHOL} < 0.5$, escalating packing (i.e., increasing Π) intensifies the repulsive interactions between DPPE and CHOL for $X_{CHOL} > 0.5$.

4.2. Interfacial dilatational rheology

Having identified key differences in the formation and thermodynamics of DPPC-CHOL versus DPPE-CHOL monolayers, which are attributed to variations in phospholipid headgroups, interfacial dilatational rheology measurements were conducted to further scrutinize the resultant alterations in the material properties of the monolayer. Utilizing oscillating pendant drops, sinusoidal $A(t)$ and resulting $\gamma(t)$ data were collected for DPPC-CHOL and DPPE-CHOL monolayers at X_{CHOL} = 0, 0.2, 0.5, 0.8 and 1, and at Π values ranging from 5 to 40 mN/m at increments of 5 mN/m, as detailed in the Materials and Methods section. Two representative plots of raw $A(t)$ and $\gamma(t)$ are shown in Figs. 6A and B for DPPE at Π = 30 and 40 mN/m. Additional plots for other monolayers are available in the supplementary material (**Figs. S2-S28**). In Fig. 6A, it is clear that there is a positive phase shift (ϕ) between γ and A, signifying that the rheological response can be described by both an elastic (storage) modulus (E') and viscous (loss) modulus (E''), where the latter can be represented as $E'' = \kappa/2\pi f$, with κ denoting a dilatational viscosity.

Interestingly, for both DPPC and DPPE at Π = 40 mN/m, a slightly negative ϕ was observed as shown in Fig. 6B for DPPE and **Fig. S7** for DPPC. Negative ϕ during oscillating dilatational rheology measurements has been reported in previous studies [52,58–64], and when applying Eq. 6 to these datasets it indicates the dilatational viscosity κ is negative. A negative viscosity lacks physical significance, but the presence of a negative ϕ between surface area (A) and measured γ constitutes an empirical observation that demands further discussion. Due to the non-spherical nature of a pendant drop, the changes in the surface area during volumetric oscillation will not be purely dilatational. Similar measurements conducted using symmetric oscillating barriers on a Langmuir trough do not result in purely dilatational deformation [65]. If we can reasonably assume that the film is unable to resist any shear deformation, then employing the Young-Laplace equation (Eq. 5) to measure γ and using Eq. 6 to calculate the dilatational moduli would be satisfactory [50]. However, if the film is capable of resisting shear deformation, the application of both Eq. 5 and Eq. 6 potentially becomes problematic, as they assume purely dilatational deformation. It is known that when a film exhibits strong enough shear resistance, the added stresses produce a drop shape that cannot be described by the Young-Laplace equation. In such cases, additional constitutive models [66] or a modified experimental apparatus that is capable of directly measuring capillary pressure [67] have been used to measure the anisotropic surface tensions. In our measurements, however, the drop shapes did not deviate from that of a Young-Laplace drop shape. This does not exclude the possibility of the film having some shear resistance, but only means the added stresses are not significant enough to produce a non-Young-Laplace shape. Indeed, in a study of simulated oscillating pendant drops [50], the authors used films that could resist both dilatational and shear deformation and the resulting drop shapes fit well to

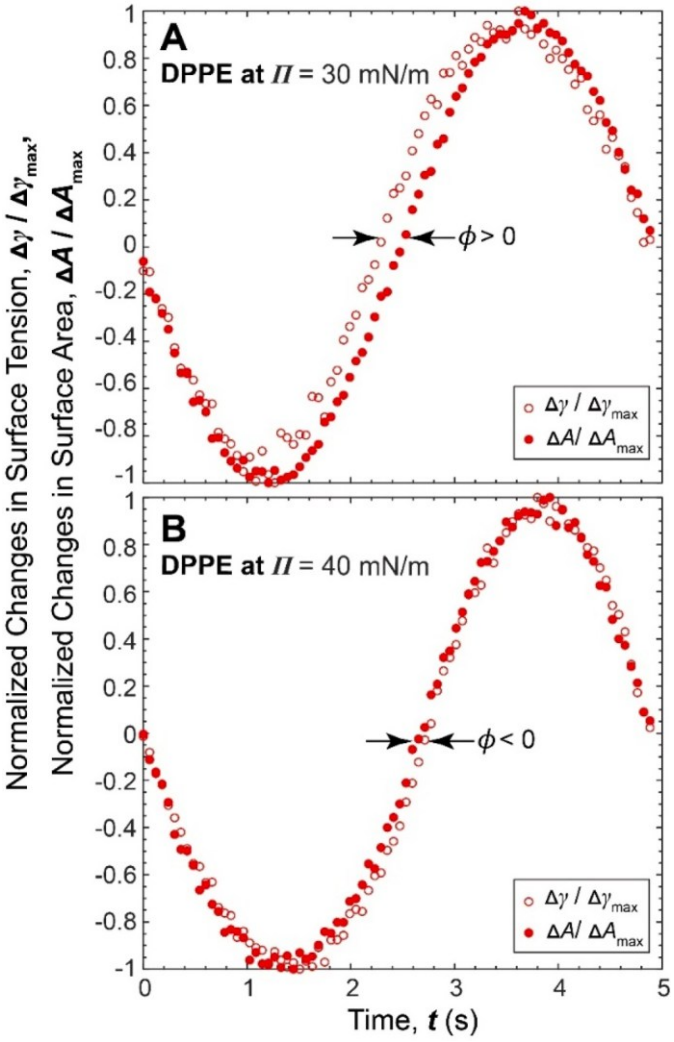

Fig 6. Plots of $\Delta\gamma/\Delta\gamma_{max}$ and $\Delta A/\Delta A_{max}$ versus t for one period at f = 0.2 Hz for DPPE are shown for **(A)** Π = 30 mN/m and **(B)** Π = 40 mN/m. The phase shift ϕ is annotated, being negative at Π = 30 mN/m and positive at Π = 40 mN/m. Data shown is from a single period of a total of 5-10 oscillation cycles performed for each measurement.

the Young-Laplace equation. Thus, the measured surface tension from fitting the Young-Laplace equation in these simulations was considered an "apparent surface tension" and denoted as γ_{app}. When fitting Eq. 6 to the simulated γ_{app} (t) and $A(t)$ results, the authors did in fact observe a negative ϕ when the shear viscosity η was large enough relative to κ. Therefore, a plausible explanation for our observation of a negative ϕ is that the films do have some shear resistance and for DPPC and DPPE at Π = 40 mN/m the ratio η/κ is large enough that ϕ becomes negative.

Applying the above reasoning implies that care must be exercised when interpreting dilatational interfacial rheology measurements of lipid monolayers on pendant drops. To accommodate this point, Eq. 6 has been fitted to our γ (t) and $A(t)$ experimental data to determine the corresponding dilatational modulus $|E|$ and phase angle ϕ, which are plotted in Fig. 7, averaged over the frequency range $0.1 \le f \le 1$ Hz. Comprehensive results of the moduli versus f are provided in the supplementary material (**Figs. S29-S37**). We begin our interpretation of the rheological results with the single-lipid monolayers, DPPC (-◦-), DPPE (-●-), and CHOL (-●-), represented by color-coordinated thick solid lines as shown in Fig. 7. In Fig. 7A, CHOL monolayers exhibit a significantly higher $|E|$ compared to both DPPC and DPPE ones, owing to its

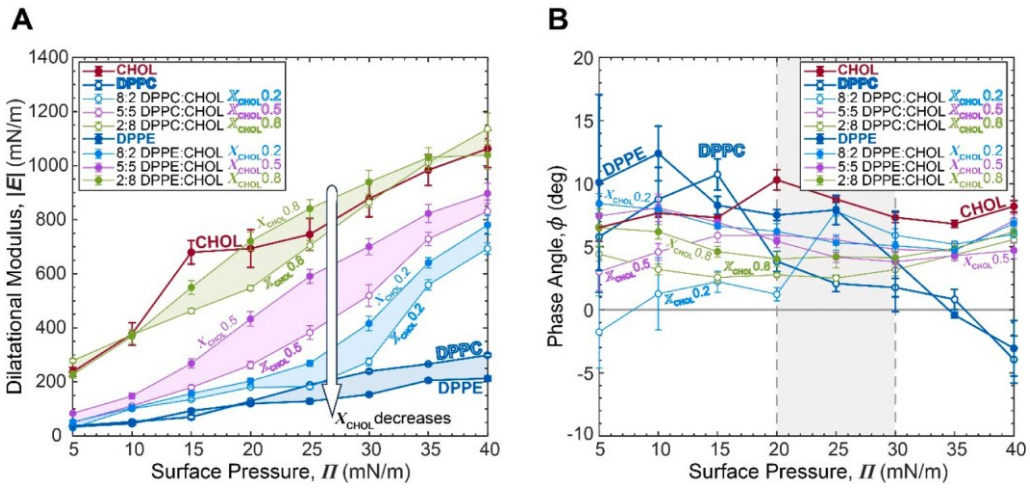

Fig. 7. The **(A)** dilatational modulus $|E|$ and **(B)** phase angle ϕ are plotted versus surface pressure for DPPC-CHOL and DPPE-CHOL monolayers. Error bars represent ± one standard deviation based on moduli measured between f = 0.1 and 1 Hz.

rigid molecular structure and ability to form a densely packed film [2]. In a comparative analysis between the pure DPPC and DPPE monolayers, DPPC consistently displays a higher $|E|$ than DPPE with the exception of the case at Π = 15 mN/m. This phenomenon can be attributed to the greater hydration of the PE headgroup in DPPE, which results in its increased immersion in the aqueous subphase relative to DPPC, thereby diminishing monolayer cohesion [19]. The exception at Π = 15 mN/m approximately corresponds to the phase transition from a liquid-expanded to liquid-condensed monolayer in DPPC (See Fig. 3), during which the monolayer can sustain substantial changes in surface area without a considerable effect on Π.

In Fig. 7B, the phase angles for all three single-lipid monolayers when Π < 20 mN/m are similar and between approximately $5^o < \phi < 10^o$. While, for CHOL (-●-), ϕ remains roughly constant over the full range of Π, ϕ starts to drop for both DPPC (-◦-) and DPPE (-●-) above Π = 20 mN/m, which roughly translates to a less fluid monolayer. In the range of 20 mN/m ≤Π ≤ 30 mN/m (shaded in light grey in Fig. 7B), DPPE-CHOL monolayers (solid circles) have a larger ϕ compared to the case of DPPC-CHOL monolayers (blank circles), suggesting between the two phospholipids, monolayers with DPPE are more fluid in this range which again can be ascribed to the reduced cohesion due to increased hydration of the PE headgroup. Above Π = 35 mN/m, both monolayers exhibit a negative ϕ. As discussed earlier, the negative ϕ strongly suggests these monolayers exhibit some shear resistance at Π = 40 mN/m, indicating that Eq. 6 is not suitable to describe the interfacial rheology of these monolayers at this pressure.

The addition of CHOL to DPPC and DPPE monolayers substantially affects the dilatational rheology, and indeed we see that the change in PE versus PC headgroup has a significant effect on the resulting moduli. In fact, while DPPC generally exhibited a larger $|E|$ than DPPE, mixed DPPE-CHOL monolayers generally exhibit a larger $|E|$ than DPPC-CHOL monolayers (See Fig. 7(A)). To more clearly visualize this and to facilitate discussion, we define the relative difference in the dilatational modulus between DPPC-CHOL and DPPE-CHOL monolayers, $\Delta|E|$, as:

$$\Delta|E| = \frac{|E|_{PC} - |E|_{PE}}{|E|_{PE}}, \tag{11}$$

where a positive $\Delta|E|$ indicates the DPPC-containing monolayer has a larger $|E|$ and vice versa. The quantity $\Delta|E|$ is plotted versus both Π (Fig. 8A) and X_{CHOL} (Fig. 8B). For $X_{CHOL} > 0$, DPPE-CHOL monolayers have a significantly larger $|E|$, in some cases approaching 70% larger. The difference is greatest primarily for X_{CHOL}=0.5 (See -★- in Fig. 8A). As discussed throughout, the PE headgroup is more easily hydrated than PC, which explains the reduced $|E|$ in DPPE compared to the case of DPPC. However, CHOL has been shown to cause dehydration when present in phospholipid monolayers [24]. For both DPPC-CHOL and DPPE-CHOL monolayers, this dehydration coupled with

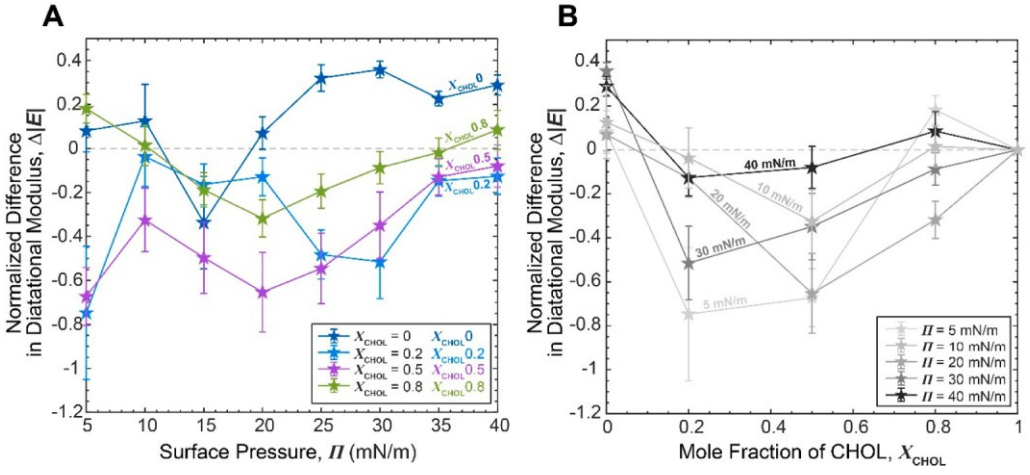

Fig. 8. Plots of the normalized difference between $|E|$ ($\Delta|E|$, See Eqn. 11) for DPPC-CHOL and DPPE-CHOL monolayers are shown as functions of **(A)** Π and **(B)** X_{CHOL}. Error bars are based on the standard deviations shown in Fig. 7.

inter-headgroup hydrogen bonding and hydrophobic interactions would increase monolayer cohesion, resulting in elevated $|E|$. In DPPE-CHOL monolayers, however, the inter-headgroup hydrogen bonding between the DPPE lipids is stronger, attributed to the PE's dual role as a hydrogen bond donor and acceptor. Consequently, the CHOL-induced dehydration of the monolayer amplifies the cohesion between DPPE lipids, leading to the larger $|E|$ compared to its DPPC-CHOL counterpart. At X_{CHOL} = 0.8, the difference in $|E|$ for DPPC- CHOL and DPPE-CHOL monolayers diminishes, as depicted in Fig. 8. This transition coincides with the CHOL-induced monolayer expansion (see Fig. 4B) and a shift to positive ΔG_{ex} (refer to Fig. 5B). Despite the immiscibility of CHOL in DPPE at these high mole fractions and the probable presence of distinct DPPE-rich domains, the dilatational modulus surpasses that of DPPC-CHOL monolayers containing the same amount of CHOL.

5. Conclusions

In the present work, we have compared the monolayer formation and interfacial dilatational rheology of two binary lipid systems, DPPC-CHOL and DPPE-CHOL, where the only difference was the phospholipid headgroup, phosphatidylcholine (PC) versus phosphatidylethanolamine (PE). Both of these headgroups are zwitterionic, with the major differences being the slightly smaller size and increased hydration of PE compared to PC. Using pendant drops, both surface pressure-area (Π-A) isotherms and dilatational rheological properties were measured.

In the realm of monolayer formation, our investigation delineates the distinct behaviors exhibited by CHOL in two contrasting environments: DPPC and DPPE monolayers. Notably, when integrated into DPPC monolayers, CHOL exerted a condensing effect at all mole fractions studied. In contrast, CHOL had a condensing effect in DPPE monolayers only for $X_{CHOL} < 0.5$, above which CHOL had an expanding effect on the monolayer. This more complicated behavior, which has been reported once before [35], agrees with observations that increased CHOL in DPPE monolayers tends to produce CHOL-poor domains [18]. An extensive analysis of both the excess mean molecular areas and the Gibbs energy of mixing (ΔG_{ex}) substantiates the interpretation that the stronger inter-headgroup hydrogen bonding between DPPE lipids favors this immiscibility at elevated CHOL concentrations.

We have also reported, for the first time, interfacial dilatational rheology results for mixed DPPE-CHOL monolayers, alongside comprehensive comparisons with DPPC-CHOL counterparts, at varying X_{CHOL} and Π. The analyses of the Π-A isotherm and ΔG_{ex} outcomes reveal significant distinctions in the rheological characteristics between DPPC-CHOL and DPPE-CHOL binary systems: (i) The enhanced hydration propensity of DPPE headgroups generally fosters less cohesive, softer monolayers compared to the case of DPPC. (ii) However, the integration of CHOL leads to stiffer DPPE-CHOL monolayers than DPPC-CHOL, particularly at X_{CHOL}= 0.2 and 0.5. We hypothesize that this reversal, where DPPE-containing monolayers become stiffer than DPPC-containing monolayers, is mediated by the synergistic effects of CHOL-induced monolayer dehydration and robust DPPE-DPPE inter-headgroup hydrogen bonding. (iii) At high CHOL concentrations ($X_{CHOL} \geq$ 0.8), the difference in $|E|$ between DPPE-CHOL and DPPC-CHOL monolayers diminishes, aligning with the calculated positive ΔG_{ex}, indicative of net repulsion in DPPE-CHOL monolayers. In this regime, despite the formation of distinct CHOL-poor domains in DPPE-CHOL monolayers, the DPPE-CHOL monolayers still generally maintain a higher rigidity compared to the more miscible DPPC-CHOL monolayers.

For DPPC and DPPE at high Π, we also measured negative phase shifts between $A(t)$ and $\gamma(t)$ at high Π. This unexpected result has been observed by others for different materials [52,58–64], and is plausibly explained by the presence of simultaneous dilatation and shear deformation as well as a monolayer that is capable of both dilatational and shear resistance [50]. This observation highlights the complex behavior of these monolayers and the difficulty in determining these interfacial rheological properties.

In conclusion, despite the challenges in measuring interfacial rheological properties, clear differences in the rheological behavior between DPPC-CHOL and DPPE-CHOL monolayers were established, attributable to the differences in the phospholipid headgroup. Our study highlights the importance of investigating the complex interactions between lipids and cholesterol in monolayers and membranes and demonstrates the power of combining monolayer formation and interfacial rheology techniques to gain insights into these systems. These findings underscore the significant influence of lipid monolayer composition on monolayer formation and material properties and highlight the complex interplay between lipid-lipid and lipid-cholesterol interactions in determining the structural and mechanical properties of biological membranes. Therefore, we believe the insights gained from this work can serve as a foundation for future studies exploring a wider range of lipid compositions and environmental conditions, with the ultimate goal of developing a comprehensive understanding of the structure-function relationships in biological membranes, potentially also leading to the development of novel biomimetic materials and drug delivery systems.

CRediT authorship contribution statement

Andrew R. White: Writing – original draft, Methodology, Investigation, Formal analysis. **Monica Iepure:** Methodology, Investigation, Formal analysis. **Jonathan Arredondo:** Methodology, Investigation. **Maryam Darwish:** Methodology, Investigation. **Chidubem Onyeagoro:** Investigation. **Younjin Min:** Writing – review & editing, Visualization, Validation, Supervision, Project administration, Methodology, Funding acquisition, Conceptualization.

Declaration of competing interest

The authors declare that they have no known competing financial interests or personal relationships that could have appeared to influence the work reported in this paper.

Acknowledgements

This research was supported by the National Science Foundation under award numbers CMMI (Civil, Mechanical & Manufacturing Innovation) – 1826250 and CBET (Chemical, Bioengineering, Environmental and Transport Systems) – 2040301.

Supplementary materials

Supplementary material associated with this article can be found, in the online version, at doi:10.1016/j.surfin.2024.105294.

Data availability

Data will be made available on request.

References

[1] G. Liebisch, E. Fahy, J. Aoki, E.A. Dennis, T. Durand, C.S. Ejsing, M. Fedorova, I. Feussner, W.J. Griffiths, H. Ko¨feler, Update on LIPID MAPS classification, nomenclature, and shorthand notation for MS-derived lipid structures, J. Lipid Res. 61 (2020) 1539–1555.

[2] H. Ohvo-Rekila¨, B. Ramstedt, P. Leppima¨ki, J.P. Slotte, Cholesterol interactions with phospholipids in membranes, Prog. Lipid Res. 41 (2002) 66–97.

[3] Y. Min, Phase dynamics and domain interactions in biological membranes, Curr. Opin. Chem. Eng. 15 (2017) 76–83.
[4] G.W. Feigenson, Phase behavior of lipid mixtures, Nat. Chem. Biol. 2 (2006) 560–563.
[5] D. Lingwood, K. Simons, Lipid rafts as a membrane-organizing principle, Science (1979) (2010), https://doi.org/10.1126/science.1174621.
[6] T. Ro´g, I. Vattulainen, Cholesterol, sphingolipids, and glycolipids: what do we know about their role in raft-like membranes? Chem. Phys. Lipids 184 (2014) 82–104.
[7] A.S.B. Olsen, N.J. Færgeman, Sphingolipids: membrane microdomains in brain development, function and neurological diseases, Open. Biol. 7 (2017) 170069.
[8] Y. Min, K. Kristiansen, J.M. Boggs, C. Husted, J. a Zasadzinski, J. Israelachvili, Interaction forces and adhesion of supported myelin lipid bilayers modulated by myelin basic protein, Proc. Natl. Acad. Sci. u S. a 106 (2009) 3154–3159, https://doi.org/10.1073/pnas.0813110106.
[9] Y. Min, T.F. Alig, D.W. Lee, J.M. Boggs, J.N. Israelachvili, J.A. Zasadzinski, Critical and off-critical miscibility transitions in model extracellular and cytoplasmic myelin lipid monolayers, Biophys. J. 100 (2011) 1490–1498.
[10] W. Szlasa, I. Zendran, A. Zalesin´ska, M. Tarek, J. Kulbacka, Lipid composition of the cancer cell membrane, J. Bioenerg. Biomembr. (2020) 1–22.
[11] A.C. Alves, D. Ribeiro, C. Nunes, S. Reis, Biophysics in cancer: The relevance of drug-membrane interaction studies, Biochimica et Biophysica Acta (BBA)-Biomembranes 1858 (2016) 2231–2244.
[12] S. Beloribi-Djefaflia, S. Vasseur, F. Guillaumond, Lipid metabolic reprogramming in cancer cells, Oncogenesis. 5 (2016) e189.
[13] J.E. Vance, Phospholipid synthesis and transport in mammalian cells, Traffic. 16 (2015) 1–18.
[14] Y. Min, M. Akbulut, K. Kristiansen, Y. Golan, J. Israelachvili, The role of interparticle and external forces in nanoparticle assembly, Nat. Mater. (2008), https://doi.org/10.1038/nmat2206.
[15] Y. Min, N. Pesika, J. Zasadzinski, J. Israelachvili, Studies of bilayers and vesicle adsorption to solid substrates: development of a miniature streaming potential apparatus (SPA), Langmuir. 26 (2010) 8684–8689.
[16] T.H. Anderson, Y. Min, K.L. Weirich, H. Zeng, D. Fygenson, J.N. Israelachvili, Formation of supported bilayers on silica substrates, Langmuir. 25 (2009) 6997–7005.
[17] M. Dyck, P. Krüger, M. Lo¨sche, Headgroup organization and hydration of methylated phosphatidylethanolamines in Langmuir monolayers, Physical Chemistry Chemical Physics 7 (2005) 150–156.
[18] T.P.W. McMullen, R.N.A.H. Lewis, R.N. McElhaney, Calorimetric and spectroscopic studies of the effects of cholesterol on the thermotropic phase behavior and organization of a homologous series of linear saturated phosphatidylethanolamine bilayers, Biochimica et Biophysica Acta (BBA)-Biomembranes 1416 (1999) 119–134.
[19] N. Anton, P. Saulnier, F. Boury, F. Foussard, J.-P. Benoit, J.E. Proust, The influence of headgroup structure and fatty acyl chain saturation of phospholipids on monolayer behavior: a comparative rheological study, Chem. Phys. Lipids 150 (2007) 167–175.
[20] G.A. Pantelopulos, J.E. Straub, Regimes of complex lipid bilayer phases induced by cholesterol concentration in MD simulation, Biophys. J. 115 (2018) 2167–2178.
[21] H. Orlikowska-Rzeznik, J. Versluis, H.J. Bakker, L. Piatkowski, Cholesterol Changes Interfacial Water Alignment in Model Cell Membranes, J. Am. Chem. Soc. (2024).
[22] S.A. Pandit, D. Bostick, M.L. Berkowitz, Complexation of phosphatidylcholine lipids with cholesterol, Biophys. J. 86 (2004) 1345–1356.
[23] K. Shikata, K. Kasahara, N.M. Watanabe, H. Umakoshi, K. Kim, N. Matubayasi, ArXiv Preprint, 2024.
[24] G. M'Baye, Y. M´ely, G. Duportail, A.S. Klymchenko, Liquid ordered and gel phases of lipid bilayers: fluorescent probes reveal close fluidity but different hydration, Biophys. J. 95 (2008) 1217–1225.
[25] T.-H. Chou, C.-H. Chang, Thermodynamic behavior and relaxation processes of mixed DPPC/cholesterol monolayers at the air/water interface, Colloids. Surf. B Biointerfaces. 17 (2000) 71–79.
[26] K. Gong, S.-S. Feng, M.L. Go, P.H. Soew, Effects of pH on the stability and compressibility of DPPC/cholesterol monolayers at the air–water interface, Colloids. Surf. a Physicochem. Eng. Asp. 207 (2002) 113–125.
[27] M. Kodama, O. Shibata, S. Nakamura, S. Lee, G. Sugihara, A monolayer study on three binary mixed systems of dipalmitoyl phosphatidyl choline with cholesterol, cholestanol and stigmasterol, Colloids. Surf. B Biointerfaces. 33 (2004) 211–226.
[28] P. Wydro, K. Ha¸c-Wydro, Thermodynamic description of the interactions between lipids in ternary Langmuir monolayers: the study of cholesterol distribution in membranes, J. Phys. Chem. B 111 (2007) 2495–2502.
[29] T. Miyoshi, S. Kato, Detailed analysis of the surface area and elasticity in the saturated 1, 2-diacylphosphatidylcholine/cholesterol binary monolayer system, Langmuir. 31 (2015) 9086–9096.
[30] G.C.M. Ruiz, W.M. Pazin, L.F. do Carmo Morato, O.N. Oliveira Jr, C.J. L. Constantino, Correlating mono-and bilayers of lipids to investigate the pronounced effects of steroid hormone 17α-ethynylestradiol on membrane models of DPPC/cholesterol, J. Mol. Liq. (2020) 113324.
[31] J. Min˜ones Jr, S. Pais, J. Min˜ones, O. Conde, P. Dynarowicz-Łątka, Interactions between membrane sterols and phospholipids in model mammalian and fungi cellular membranes—A Langmuir monolayer study, Biophys. Chem. 140 (2009) 69–77.
[32] D. Gidalevitz, DPPC and cholesterol form crystalline structure responsible for pulmonary surfactant resistance to collapse, Biophys. J. 123 (2024) 95a.
[33] J. Kurniawan, T.L. Kuhl, Characterization of solid-supported dipalmitoylphosphatidylcholine membranes containing cholesterol, Langmuir. 31 (2015) 2527–2532.
[34] P. Wydro, The interactions between cholesterol and phospholipids located in the inner leaflet of humane erythrocytes membrane (DPPE and DPPS) in binary and ternary films—The effect of sodium and calcium ions, Colloids. Surf. B Biointerfaces. 82 (2011) 209–216.
[35] B. Korchowiec, M. Paluch, Y. Corvis, E. Rogalska, A Langmuir film approach to elucidating interactions in lipid membranes: 1, 2-dipalmitoyl-sn-glycero-3-phosphoethanolamine/cholesterol/metal cation systems, Chem. Phys. Lipids 144 (2006) 127–136.
[36] K. Dopierała, K. Karwowska, A.D. Petelska, K. Prochaska, Thermodynamic, viscoelastic and electrical properties of lipid membranes in the presence of astaxanthin, Biophys. Chem. 258 (2020) 106318.
[37] M. Vrˆanceanu, K. Winkler, H. Nirschl, G. Leneweit, Surface rheology and phase transitions of monolayers of phospholipid/cholesterol mixtures, Biophys. J. 94 (2008) 3924–3934.
[38] A. Jyoti, R.M. Prokop, A.W. Neumann, Manifestation of the liquid-expanded/liquid-condensed phase transition of a dipalmitoylphosphatidylcholine monolayer at the air-water interface, Colloids. Surf. B Biointerfaces. 8 (1997) 115–124.
[39] R. Wüstneck, N. Wüstneck, D.O. Grigoriev, U. Pison, R. Miller, Stress relaxation behaviour of dipalmitoyl phosphatidylcholine monolayers spread on the surface of a pendant drop, Colloids. Surf. B Biointerfaces. 15 (1999) 275–288.
[40] M. Vrˆanceanu, K. Winkler, H. Nirschl, G. Leneweit, Surface rheology of monolayers of phospholipids and cholesterol measured with axisymmetric drop shape analysis, Colloids. Surf. a Physicochem. Eng. Asp. 311 (2007) 140–153.
[41] N. Anton, P. Pierrat, L. Lebeau, T.F. Vandamme, P. Bouriat, A study of insoluble monolayers by deposition at a bubble interface, Soft. Matter. 9 (2013) 10081–10091.
[42] F.C. Goodrich, Molecular interaction in mixed monolayers, Proc. 2nd Int. Congr. Surface Act 15 (1957) 85.
[43] H. Koolivand, S. Mazinani, F. Sharif, Surface activity of N-graphene quantum dot in presence of CTAB surfactant, Surf. Interfaces 37 (2023) 102714.
[44] K. Wojciechowski, I. Jurek, I. Go´ral, M. Campana, T. Geue, T. Gutberlet, Surface-active extracts from plants rich in saponins–effect on lipid mono-and bilayers, Surfaces and Interfaces 27 (2021) 101486.
[45] S.M.I. Saad, A.W. Neumann, Axisymmetric drop shape analysis (ADSA): an outline, Adv. Colloid. Interface Sci. 238 (2016) 62–87.
[46] M. Hoorfar, A.W. Neumann, Recent progress in axisymmetric drop shape analysis (ADSA), Adv. Colloid. Interface Sci. 121 (2006) 25–49.
[47] N.J. Alvarez, L.M. Walker, S.L. Anna, A non-gradient based algorithm for the determination of surface tension from a pendant drop: Application to low Bond number drop shapes, J. Colloid. Interface Sci. 333 (2009) 557–562.
[48] A.R. White, T. Ward, Pattern search methods for pendant drops: Algorithms for rapid determination of surface tension and surfactant transport parameters, Colloids. Surf. a Physicochem. Eng. Asp. 485 (2015) 1–10.
[49] A. Yeung, T. Dabros, J. Masliyah, Dissipative Interfaces and Departures from the Young– Laplace Equation, Langmuir. 13 (1997) 6597–6606.
[50] A. Yeung, L. Zhang, Shear effects in interfacial rheology and their implications on oscillating pendant drop experiments, Langmuir. 22 (2006) 693–701.
[51] R. Myrvold, F.K. Hansen, Surface elasticity and viscosity from oscillating bubbles measured by automatic axisymmetric drop shape analysis, J. Colloid. Interface Sci. 207 (1998) 97–105.
[52] F. Ravera, G. Loglio, V.I. Kovalchuk, Interfacial dilational rheology by oscillating bubble/drop methods, Curr. Opin. Colloid. Interface Sci. 15 (2010) 217–228.
[53] M.D. Reichert, N.J. Alvarez, C.F. Brooks, A.M. Grillet, L.A. Mondy, S.L. Anna, L. M. Walker, The importance of experimental design on measurement of dynamic interfacial tension and interfacial rheology in diffusion-limited surfactant systems, Colloids. Surf. a Physicochem. Eng. Asp. 467 (2015) 135–142.
[54] M. Jurak, Thermodynamic aspects of cholesterol effect on properties of phospholipid monolayers: Langmuir and Langmuir–Blodgett monolayer study, J. Phys. Chem. B 117 (2013) 3496–3502.
[55] P. Wydro, K. Ha¸c-Wydro, Thermodynamic description of the interactions between lipids in ternary Langmuir monolayers: the study of cholesterol distribution in membranes, J. Phys. Chem. B 111 (2007) 2495–2502.
[56] H. Ohvo-Rekil˜a, B. Ramstedt, P. Leppim˜aki, J.P. Slotte, Cholesterol interactions with phospholipids in membranes, Prog. Lipid Res. 41 (2002) 66–97.
[57] T.P.W. McMullen, R.N. McElhaney, Differential scanning calorimetric studies of the interaction of cholesterol with distearoyl and dielaidoyl molecular species of phosphatidylcholine, phosphatidylethanolamine, and phosphatidylserine, Biochemistry 36 (1997) 4979–4986.
[58] V.E. Cuenca, M. Ferna? ndez Leyes, R.D. o Falcone, N.M. Correa, D. Langevin, H. n Ritacco, Interfacial Dynamics and Its Relations with? Negative? Surface Viscosities Measured at Water? Air Interfaces Covered with a Cationic Surfactant, Langmuir. 35 (2019) 8333–8343.
[59] D. Wu, Y. Feng, G. Xu, Y. Chen, X. Cao, Y. Li, Dilational rheological properties of gemini surfactant 1, 2-ethane bis (dimethyl dodecyl ammonium bromide) at air/water interface, Colloids. Surf. a Physicochem. Eng. Asp. 299 (2007) 117–123.

[60] K. Fang, G. Zou, P. He, Dynamic viscoelastic properties of spread monostearin monolayer in the presence of glycine, J. Colloid. Interface Sci. 266 (2003) 407–414.
[61] Y.-Y. Wang, Y.-H. Dai, L. Zhang, L. Luo, Y.-P. Chu, S. Zhao, M.-Z. Li, E.-J. Wang, J.-Y. Yu, Hydrophobically modified associating polyacrylamide solutions: Relaxation processes and dilational properties at the oil– water interface, Macromolecules. 37 (2004) 2930–2937.
[62] F. Monroy, J.G. Kahn, D. Langevin, Dilational viscoelasticity of surfactant monolayers, Colloids. Surf. a Physicochem. Eng. Asp. 143 (1998) 251–260.
[63] J. Giermanska-Kahn, F. Monroy, D. Langevin, Negative effective surface viscosities in insoluble fatty acid monolayers: Effect of phase transitions on dilational viscoelasticity, Phys. Rev. e 60 (1999) 7163.
[64] E.M. Freer, H. Wong, C.J. Radke, Oscillating drop/bubble tensiometry: effect of viscous forces on the measurement of interfacial tension, J. Colloid. Interface Sci. 282 (2005) 128–132.
[65] M. Pepicelli, T. Verwijlen, T.A. Tervoort, J. Vermant, Characterization and modelling of Langmuir interfaces with finite elasticity, Soft. Matter. 13 (2017) 5977–5990.
[66] S. Knoche, D. Vella, E. Aumaitre, P. Degen, H. Rehage, P. Cicuta, J. Kierfeld, Elastometry of deflated capsules: Elastic moduli from shape and wrinkle analysis, Langmuir. 29 (2013) 12463–12471.
[67] K.D. Danov, R.D. Stanimirova, P.A. Kralchevsky, K.G. Marinova, N.A. Alexandrov, S.D. Stoyanov, T.B.J. Blijdenstein, E.G. Pelan, Capillary meniscus dynamometry–Method for determining the surface tension of drops and bubbles with isotropic and anisotropic surface stress distributions, J. Colloid. Interface Sci. 440 (2015) 168–178.